

RESEARCH

Open Access



Effect of APOE ϵ 4 on multimodal brain connectomic traits: a persistent homology study

Jin Li¹, Chenyuan Bian^{1,3}, Dandan Chen¹, Xianglian Meng², Haoran Luo¹, Hong Liang^{1*} and Li Shen^{3*}  on behalf of for the Alzheimer's Disease Neuroimaging Initiative

From The International Conference on Intelligent Biology and Medicine (ICIBM) 2020 Virtual. 9-10 August 2020

*Correspondence:

lh@hrbeu.edu.cn;
li.shen@penmedicine.
upenn.edu

¹ College of Automation,
Harbin Engineering
University, 145 Nantong
Street, Harbin 150001,
Heilongjiang, China

³ Department of Biostatistics,
Epidemiology
and Informatics, Perelman
School of Medicine,
University of Pennsylvania,
B306 Richards Building, 3700
Hamilton Walk, Philadelphia,
PA 19104, USA

Full list of author information
is available at the end of the
article

Abstract

Background: Although genetic risk factors and network-level neuroimaging abnormalities have shown effects on cognitive performance and brain atrophy in Alzheimer's disease (AD), little is understood about how apolipoprotein E (APOE) ϵ 4 allele, the best-known genetic risk for AD, affect brain connectivity before the onset of symptomatic AD. This study aims to investigate APOE ϵ 4 effects on brain connectivity from the perspective of multimodal connectome.

Results: Here, we propose a novel multimodal brain network modeling framework and a network quantification method based on persistent homology for identifying APOE ϵ 4-related network differences. Specifically, we employ sparse representation to integrate multimodal brain network information derived from both the resting state functional magnetic resonance imaging (rs-fMRI) data and the diffusion-weighted magnetic resonance imaging (dw-MRI) data. Moreover, persistent homology is proposed to avoid the ad hoc selection of a specific regularization parameter and to capture valuable brain connectivity patterns from the topological perspective. The experimental results demonstrate that our method outperforms the competing methods, and reasonably yields connectomic patterns specific to APOE ϵ 4 carriers and non-carriers.

Conclusions: We have proposed a multimodal framework that integrates structural and functional connectivity information for constructing a fused brain network with greater discriminative power. Using persistent homology to extract topological features from the fused brain network, our method can effectively identify APOE ϵ 4-related brain connectomic biomarkers.

Keywords: APOE ϵ 4, Brain network, Persistent homology, Alzheimer's disease



Background

Alzheimer's disease (AD) is a chronic neurodegenerative brain disease that gradually causes cognitive deterioration [1, 2]. Although studies on the specificity of disease stage is underway to identify potential biomarkers, early diagnosis of vulnerability to AD—prior to the onset of clear cognitive symptoms—is still challenging [3, 4]. In past years, neuroimaging-based techniques have been used to reveal the neuronal interaction patterns of anatomically segregated brain regions in AD via constructing brain connectome [1, 5]. However, traditional network-level neuroimaging approaches have limited ability to discriminating normal aging from early AD [6]. Neuroimaging genetics offers a promising strategy for detecting potential early biomarkers of AD and improving the understanding of neurobiological features associated with genetic polymorphisms at risk for AD [7]. In particular, apolipoprotein E (APOE) $\epsilon 4$ allele is the uppermost genetic risk factor for developing sporadic AD, which is observed in up to 50% of all AD cases [8]. We propose here a brain imaging genetics study to examine the effect of the APOE $\epsilon 4$ genotype on brain connectomic traits. Our goal is to quantify the functional and structural brain differences from the perspective of genetics in patients, who may be undergoing early neuropathological changes in the pathological cascade leading to disease. Currently, an ample number of studies [9, 10] have investigated the brain connectivity features of APOE $\epsilon 4$ carriers. These existing studies found specific and consistent alterations in brain network, especially involving decreased functional connectivity within default mode network (DMN). Particularly, most of these approaches for characterizing APOE-related network differences are based on pairwise correlation such as Pearson's correlation. Nevertheless, some studies [11, 12] have demonstrated that the neurological processes involve the interactions of many co-activated brain regions (i.e., more than two brain regions) rather than just the pairwise variant-trait associations.

To address this problem, the least absolute shrinkage and selection operator (Lasso) and sparse representation have been applied to construct a sparse brain network by considering more complex interactions among multiple co-activated brain regions [13]. However, the Lasso approaches have their own limitations. For example, most of them use a fixed regularization parameter λ that may not be optimal to control the model sparsity, which can lead to an uncertainty to quantify the sparse brain networks [14]. Moreover, another problem with Lasso is, feature extraction of sparse network needs a constructed network with precise connection strengths [15]. However, traditional Lasso method has been shown biased, and may not provide reliable estimation for building brain networks. Therefore, a subsequent connectivity strength estimation process should be performed to eliminate the shrinking effect, which naturally adds the complexity of modeling. In order to address the above limitations, a persistent homology (PH) [16–19] method is newly proposed in this work. Our novel method constructs the brain network over multiscale regularization parameter space and only focuses on the network structure (binary network) rather than connection strength (weight network) between regions. Hence, we hypothesize that the combination of PH and SR may yield a potential path to identify more sensitive brain network-level biomarkers.

Currently, a lot of brain network modeling methods only consider the neurological processes from a single modality [20], while compelling evidences have demonstrated the benefit of acquiring and fusing complementary information via different neuroimaging

modalities for accurate classification [21, 22]. Specifically, diffusion-weighted MRI (dw-MRI) has been applied to map white matter tractography that outputs structural connectivity (SC). On the other hand, resting state functional MRI (rs-fMRI) measures intrinsic functional connectivity (FC) through spontaneous fluctuations of brain activity. Joint investigation of dw-MRI and rs-fMRI data can offer a complete characterization of the brain network incorporating both structural and functional connectivity. For example, Qi et al. [23] proposed a framework for integrating the multimodal imaging data of diffusion-MRI and fMRI. Their results suggested that the multimodal fusion can effectively detect potential imaging biomarkers of working memory deficits in schizophrenia. Korthauer et al. [6] integrated rs-fMRI and dw-MRI data in a single network for investigating a functional-structural network difference in apolipoprotein E (APOE) $\epsilon 4$ carriers and non-carriers. In their study, integrating multiple neuroimaging modalities was demonstrated to be a more effective method to detect network-level biomarkers compared to conventional single modality method. Based on these findings, we hypothesize that a multimodal fusion method may further improve the statistical performance between APOE $\epsilon 4$ carriers and non-carriers.

In this paper, we focus on identifying APOE $\epsilon 4$ related differences from the perspective of brain connectome. The main methodological contributions are threefold. First, we propose a novel multimodal brain network modeling method for detecting the differences of APOE $\epsilon 4$ -associated brain connectivity. Our method integrates the multimodal information from both rs-fMRI and dw-MRI. Specifically, a generalized fused Lasso method is applied to linearly regress rs-fMRI signals (BOLD time series), and is guided by SC prior information. Second, we develop a multiscale network quantification method using PH for the proposed model. We show that after integrating the brain network information with different sparsity for each subject, PH can effectively characterize the multiscale networks via graph filtration, which overcomes the uncertainty of optimal parameter selection. To the best of our knowledge, no previous methods ever fused both multimodal brain modeling and PH into a sparse representation, upon which our novel framework is built. Third, we design a connectivity pattern identification method based on PH features. Different from the existing methods, our method can characterize the APOE $\epsilon 4$ -related specific loop structures in the brain network, which can reflect meaningful biological communication patterns. Finally, we perform our experimental study using rs-fMRI and dw-MRI data from the publicly available Alzheimer's Disease Neuroimaging Initiative (ADNI) database. We demonstrate the promise of our method over the competing methods on both statistical performance and connectivity pattern identification.

Methods

Participants

Data used in the preparation of this article were obtained from the ADNI database (adni.loni.usc.edu). In this study, APOE genotype, rs-fMRI, dw-MRI, and T1 imaging data were collected from 63 subjects, and divided into two groups: APOE $\epsilon 4$ carriers ($N=27$, 17 males and 10 females, age 63–89) and APOE $\epsilon 4$ non-carriers ($N=36$, 20 males and 16 females, age 61–87).

Genotype and neuroimaging data

For genotyping, subjects carrying at least one APOE $\epsilon 4$ allele were defined as APOE $\epsilon 4$ carriers (genotype $\epsilon 4/\epsilon 4$ and $\epsilon 4/\epsilon 3$), while subjects with the genotype $\epsilon 3/\epsilon 3$ were classified as APOE $\epsilon 4$ non-carriers. Subjects with the $\epsilon 2$ allele (including genotypes $\epsilon 2/\epsilon 2$, $\epsilon 2/\epsilon 3$, and $\epsilon 2/\epsilon 4$) were excluded in this study. For neuroimaging data, all MRI data were acquired with a Siemens 3 T scanner with the following parameters: (1) rs-fMRI data involved that TE (echo time) = 30 ms, TR (repetition time) = 3000 s, FA (flip angle) = 90 degree, slice thickness = 3.4 mm, the number of slices = 197; (2) dw-MRI data were acquired with gradient directions = 54, TE = 56 ms, TR = 7200 ms, voxel size = $2 \times 2 \times 2 \text{ mm}^3$, FA = 90 degree; (3) T1 image data were acquired with FA = 9 degree, acquisition plane = SAGITTAL, slice thickness = 1.2 mm, TE = 2.95 ms, T1 = 900 ms, TR = 2300 ms.

Data preprocessing

T1 is a structural MRI (sMRI) modality capturing brain morphometry. T1 is often used as a reference image to which dw-MRI and rs-fMRI data can be registered. After that, all three modalities are aligned to the same reference so that multimodal data analysis can be facilitated.

For rs-fMRI data, we used SPM8 (<https://www.fil.ion.ucl.ac.uk/spm/software/spm8/>) and DPABI [24] for preprocessing as follows: removing the first 10 time points; slice timing correction; spatial correction for head motion; co-registering the individual T1 image to the mean functional image after realignment by using DARTEL (a fast diffeomorphic anatomical registration algorithm to calculate the transformations from individual native space to MNI space); smoothing using Gaussian kernel with FWHM (full-width-at-half-maximum) of $4 \times 4 \times 4 \text{ mm}^3$; standardization to reduce the impact of nuisance covariates including head motion parameters, white matter signal and cerebrospinal fluid signal. For quality control, the rs-fMRI data with greater 2.5 mm and 2.5 degree in max head motion are excluded.

For dw-MRI data, we used a package called pipeline toolbox for analyzing brain diffusion images (PANDA) [25] developed based on the FMRIB Software Library (FSL, <https://fsl.fmrib.ox.ac.uk/fsl/>). Specifically, it includes estimating a brain mask using *bet* command of FSL based on b_0 image without diffusion weighting; removing the non-brain spaces by *fslroi* command; eddy-current correction; calculation for diffusion tensor metrics by *dtifit* command; deterministic white matter tractography within brain using *dti_recon* and *dti_tracker* commands of the Diffusion Toolkit (<http://trackvis.org/dtk/>). We found that the *bet* command of FSL shows better results for brain tissue extraction than PANDA, so T1 image without skull is achieved using this approach. Each subject's FA image is co-registered to its corresponding T1 image based on *flirt* in FSL for defining network nodes. For quality control, the dw-MRI data with significant distortion in co-registration with FA and T1 image or with T1 image and MNI template were excluded from the study. Of note, since T1 scans were used for jointly guiding both dw-MRI and rs-fMRI registrations, the multimodal images were registered onto a same reference template.

Multimodal brain network

The framework of multimodal brain network modeling is shown in Fig. 1a. Let us assume that we have N subjects and M regions of interest (ROIs). For each ROI, a regional mean fMRI BOLD time series is available. We suppose that the BOLD time series with respect to the i -th ROI can be denoted as $x_i = \{x_{1i}, x_{2i}, \dots, x_{Ti}\} \in R^T$, where T is the number of time points (we have 280 time points). $\beta_i = \{\beta_{1i}, \beta_{2i}, \dots, \beta_{Mi}\} \in R^M$ is the coefficient vector that represents the indices of other co-activated ROIs associated with the i -th ROI. We can estimate the whole-brain network $B = \{\beta_1, \beta_2, \dots, \beta_M\} \in R^{M \times M}$ by solving the following l_1 -norm regularization problem:

$$\min_{\beta} \frac{1}{2} \left\| x_i - \sum_{j \neq i} x_j \beta_{ji} \right\|_2^2 + \lambda_1 \sum_{j \neq i} |\beta_{ji}| \tag{1}$$

where λ_1 is a non-negative regularization parameter controlling the sparsity of the brain network. A larger λ_1 forces more coefficients to be zeros, i.e., more values in coefficient vector $\{\beta_i\}_{i=1}^M$ equal to zero, which is able to select the strongly co-activated ROIs from the i -th ROI to the other ROIs. In general, functional network estimated by rs-fMRI can measure the temporal correlation of anatomically segregated brain regions, while a structural network based on dw-MRI is formed by characterizing the white matter fiber

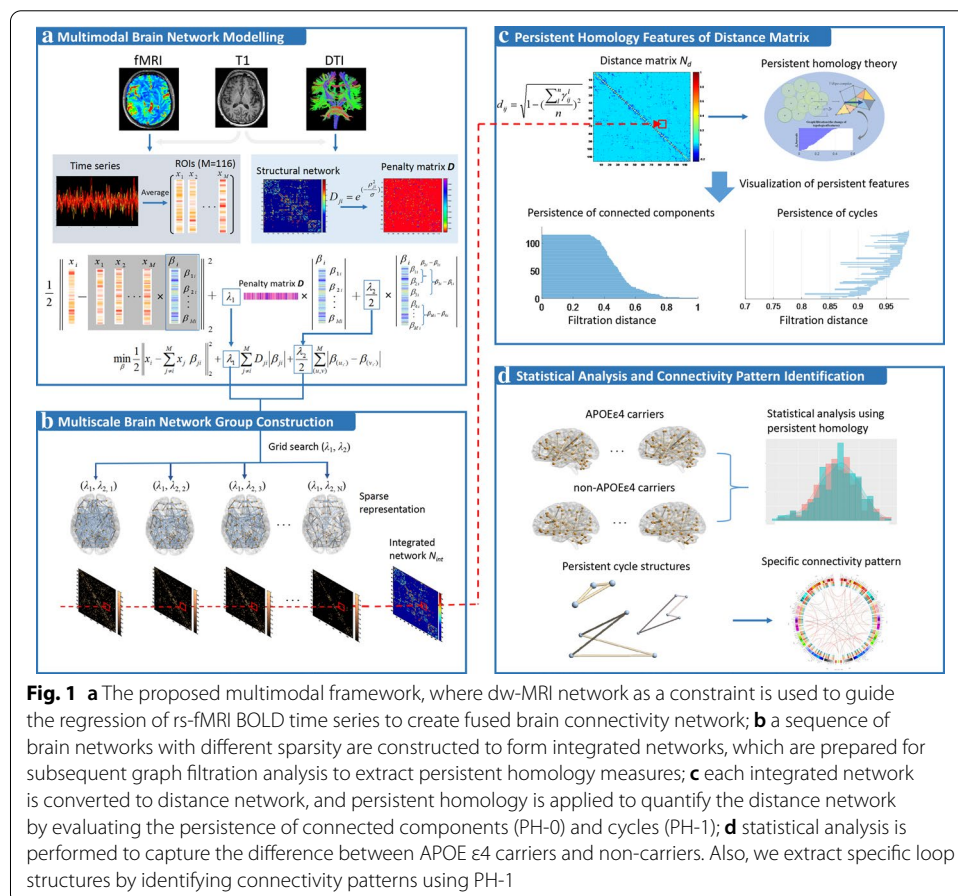


Fig. 1 **a** The proposed multimodal framework, where dw-MRI network as a constraint is used to guide the regression of rs-fMRI BOLD time series to create fused brain connectivity network; **b** a sequence of brain networks with different sparsity are constructed to form integrated networks, which are prepared for subsequent graph filtration analysis to extract persistent homology measures; **c** each integrated network is converted to distance network, and persistent homology is applied to quantify the distance network by evaluating the persistence of connected components (PH-0) and cycles (PH-1); **d** statistical analysis is performed to capture the difference between APOE ϵ 4 carriers and non-carriers. Also, we extract specific loop structures by identifying connectivity patterns using PH-1

tracts. In order to integrate these two sources of complementary information, we propose to incorporate the structural network into Eq. (1) to guide modeling of the functional brain network. Thus, a multimodal network construction can be formulated as:

$$\min_{\beta} \frac{1}{2} \left\| x_i - \sum_{j \neq i}^M x_j \beta_{ji} \right\|_2^2 + \lambda_1 \sum_{j \neq i}^M D_{ji} |\beta_{ji}| \tag{2}$$

where D_{ji} represents the structural connectivity information computed from the dw-MRI data. The neurological basis of D_{ji} is that the coupling of functional and structural connectivity can be regarded as significantly correlated with brain development. A stronger FC is likely to be attributed to a larger SC, and in turn a lower penalty to $\{\beta_i\}_{i=1}^M$. Therefore, we define the D_{ji} as an inverse proportion function of SC. In particular, we set $D_{ji} = \exp(-\rho_{ji}^2/\sigma)$ to penalize the estimated connection between the j -th and i -th ROIs, where ρ_{ji} denotes elements in the structural brain network, and σ is the average of standard variances of all subjects' structural network elements (i.e., ρ_{ji}).

Note that the aforementioned model only characterizes the extent of the influence from the i -th ROI to other ROIs, ignoring the temporal dependency among the other ROIs. Thus, we further introduce an additional source of guidance, named generalized fused Lasso, to pursue smoothness between the pairwise ROIs as follows:

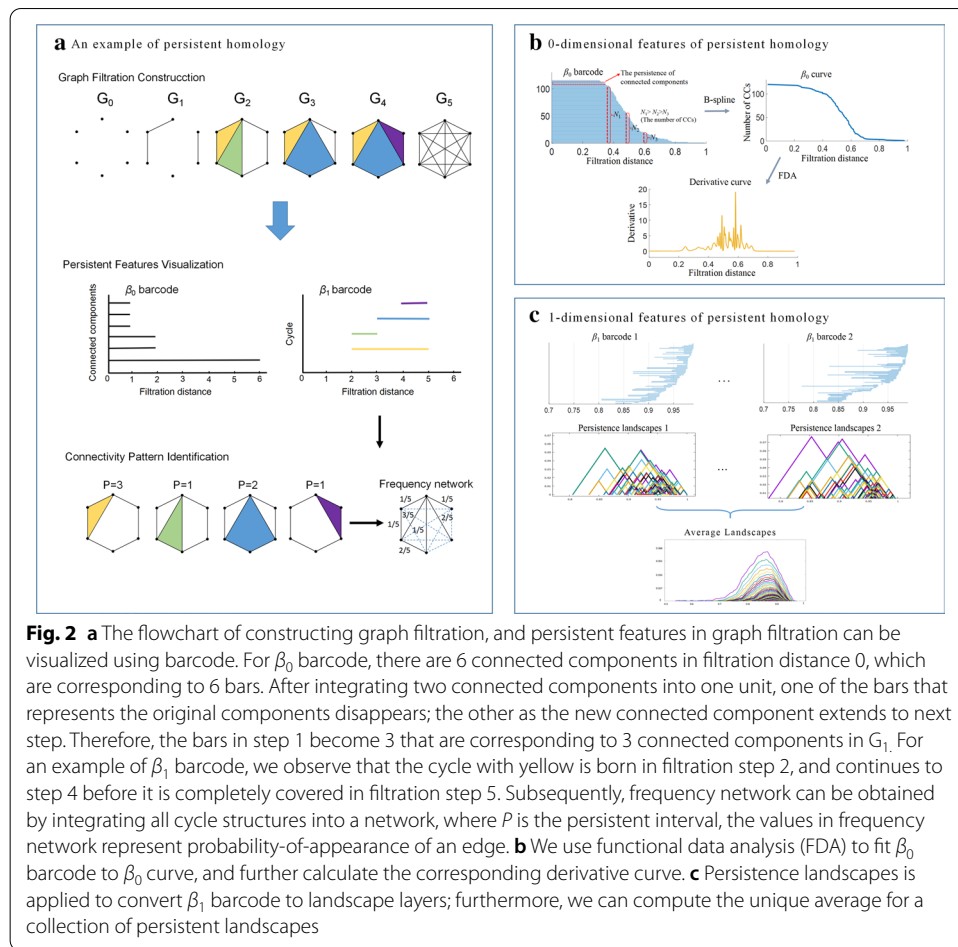
$$\min_{\beta} \frac{1}{2} \left\| x_i - \sum_{j \neq i}^M x_j \beta_{ji} \right\|_2^2 + \lambda_1 \sum_{j \neq i}^M D_{ji} |\beta_{ji}| + \frac{\lambda_2}{2} \sum_{(u,v)} |\beta_{(u,\cdot)} - \beta_{(v,\cdot)}| \tag{3}$$

where $\frac{\lambda_2}{2} \sum_{(u,v)} |\beta_{(u,\cdot)} - \beta_{(v,\cdot)}|$ is the generalized fused Lasso term, which is used to adaptively control the similarity by shrinking the difference between ROIs toward zero. Moreover, l_1 -norm regularization is used to penalize the fusion term, which results in a sparse pattern.

Persistent homology quantification

Persistent homology (PH)—a mathematical formalism from computational topology [26]—can explore the persistence of topological invariants in a network, including connected components, cycles, voids, etc. More specifically, a process called *graph filtration* generates a series of nested simplicial complexes by varying the value of a filtration parameter [27]. Furthermore, we can track the persistence over the graph filtration from the formation (birth) of a topological feature until it disappears (death) by being connected to a neighboring network (Fig. 2a). In general, we define *0-dimensional features* (PH-0) as the persistence of connected components, *1-dimensional features* (PH-1) as the persistence of cycle structures. When thinking of these persistent intervals as bars, we can construct a *barcode* using the finite multi-set of bars to record the PH features, where PH-0 is represented using β_0 barcode (Fig. 2b), PH-1 is using β_1 barcode (Fig. 2c). Particularly, we can record the cycle structures over the graph filtration, and then integrate them to a *frequency network* which contains the specific connectivity information of the network.

Because there is no definite rule to determinate the proper λ_1 and λ_2 for the proposed model in Eqs. (2, 3), it will lead to inconsistency of network structure and uncertainty of



results that follow. The problem can be remedied by using PH to perform statistical inference over every possible λ . More specifically, suppose that a group of brain networks $N_G = (N_{\lambda_1}, N_{\lambda_2}, \dots, N_{\lambda_n})$ corresponding to different regularization parameters ($\lambda_1 < \lambda_2 < \dots, < \lambda_n$) rather than a fixed parameter, we can integrate the network group into an integrated network N_{int} (see Fig. 1b). The elements in N_{int} can be defined as probability-of-appearance of an edge in the network group N_G . Assuming $\gamma = 1$ or 0 represents an edge exists or not, n is the number of networks in N_G , we use distance network N_d to convert the elements of N_{int} by $d_{ij} = \sqrt{1 - \left(\sum_l \gamma_{ij}^l / n\right)^2} \in N_d$ (see Fig. 1c). Then, a graph filtration for N_d can be constructed as follows: (1) Initial step is corresponding to the set of all brain regions; (2) Linearly increase the filtration distance ε (i.e., threshold) within the interval $[0, 1]$, where the maximum number of generated networks is set as 1000; (3) For each ε , threshold the weighted distance network N_d using $d_{ij} < \varepsilon$ to construct a binary network; (4) In the end, all brain nodes will be connected to one large unit. PH can be used to encode the graph filtration using the PH-0 and PH-1.

0-dimensional features (PH-0) We can obtain a β_0 curve by fitting the β_0 barcode using a *functional data analysis* (FDA) which can track the β_0 curve features by combining *b-spline* basis functions with proper choice of roughness penalties [28, 29] (see Fig. 2b). Mathematically, the β_0 curve function y_{β_0} can be defined as:

$$y_{\beta_0} = \sum_{k=1}^j c_k \varphi_k(t) + \varepsilon_j = \mathbf{c}^T \boldsymbol{\varphi}(t) + \varepsilon_j \tag{4}$$

where ϕ is an order four b -spline basis, and c contains the penalty coefficients, the residuals ε_j is statistically independent. However, the fitting curves are not smooth because the process simply interpolates these points with lines. The problem can be addressed by minimizing the Eq. (5), which provides a compatible between capturing important curve features and reduce computations.

$$\min F(c) = \sum_j [y_j - c^T \varphi_j]^2 + \lambda \int (c^T \varphi_j)^2 dt \tag{5}$$

where the first term on the right side is the ordinary sum of squared errors of residuals, and the second term is the measure of roughness. The smoothing parameter λ specifies the emphasis on the integration relative to the goodness of fit in the SSE. As λ approaches positive infinity, curves become less rough and converge to a straight line. A theme in functional data analysis is the possibility of also using information on the rates of change or derivatives of the curves [30], because these curves are intrinsically smooth. The derivative curve of β_0 fitting can magnify the curve’s features, thereby measuring the network difference through the curve distance measures like Cityblock and standardized Euclidean (Seuclidean) distance.

1-dimensional features (PH-1): A *persistence landscapes* method can convert the nonstandard and nonlinear 1-dimensional features to a sequence of piecewise-linear functions in Banach space, so we can use the linear vector space structures [31]. Their calculation is much faster than the corresponding barcode calculation. Given a β_1 barcode interval (b, d) with $b < d$, the piecewise linear function is defined as:

$$f_{(b,d)}(x) = \begin{cases} 0 & \text{if } x \notin (b, d) \\ x - b & \text{if } x \in (b, \frac{b+d}{2}) \\ -x + b & \text{if } x \in (\frac{b+d}{2}, d) \end{cases} \tag{6}$$

The persistence landscapes of a β_1 barcodes $\{(b_i, d_i)\}_{i=1}^n$ is a sequence of function λ_k so that λ_k is equals to the k -th largest value of $\{f_{(b_i,d_i)}(x)\}_{i=1}^n$. More specifically, for every fixed k , λ_k can be regarded as exterior contours of a group of pairwise linear functions. Statistically, the great advantage of persistence landscapes is that, it is possible to compute the unique mean landscapes for a collection of persistent landscapes by taking the average for every landscape layer [32] (see Fig. 2c). This is not possible for barcodes, as they are not elements of a Banach space. The L_p distances can be used to quantify the difference between $\lambda_k(t)$ and $\lambda'_k(t)$ corresponding to two persistent landscapes. In addition, we can not only calculate the L_p distance for $1 \leq p \leq \infty$ between the pairwise landscapes, but also between the average landscapes for two groups of persistence barcodes when analyze statistically. That allows one to compare multiple groups of β_1 barcodes by calculating the pairwise similarity between them.

Parameter selection

In the proposed multimodal modeling framework, there are two free parameters: l_1 -regularization parameter λ_1 , and fused Lasso parameter λ_2 , which control the performance of evaluation. A grid search is applied to search the optimal parameter combination. Of

note, for obtaining the sequence of networks with different sparsity, a group of regularization parameter λ_1 are selected in the range of $[0, 0.9]$ with a uniform step size. Hence, we set the total sampling number of λ_1 as a free parameter N_{λ_1} , and its candidate values for grid search are $[100, 200, \dots, 500]$. The candidate values for the fused Lasso parameter λ_2 are $[0.1, 0.2, \dots, 0.8]$. In a word, our method involves the two parameters $\{N_{\lambda_1}, \lambda_2\}$ which should be optimized for receiving the most specific difference in APOE $\epsilon 4$ -related group analysis.

Statistical analysis and comparison

For the functional network, the structural network, and the proposed multimodal network, group-level significant differences between APOE $\epsilon 4$ carriers and non-carriers are computed (Fig. 1d). A non-parametric permutation test (see Additional file 1: Appendix S1) is used to assess the statistical difference for PH measurements (i.e., PH-0 and PH-1), while the graph theory measurements [33] such as local efficiency (LE), betweenness (BET), global efficiency (GE), and clustering coefficient (CCO) are evaluated using a two-sample t-tests. Significance is determined using a level of 0.05. For subject-level network differences, we denote *distances within group* (DWG) as the distances between all pairs of subjects within a group. For example, DWG of the APOE $\epsilon 4$ carriers with 27 subjects can be a vector composed of 351 pairwise distances. Similarly, the *distances between groups* (DBG) indicate the distances between all pairs of subjects from different groups. For instance, the DBG between APOE $\epsilon 4$ carriers (27 subjects) and non-carriers (36 subjects) could consist of 972 pairwise distances. In this study, Euclidean distance is used to measure the distances in DWG and DBG. Furthermore, we compared the PH metrics and the competing graph theory metrics.

Connectivity pattern identification

We develop a connectivity pattern identification method for exploring the specific connectivity structures for APOE $\epsilon 4$ carriers and non-carriers, respectively. First, during the graph filtration, the brain regions synchronizing in a cycle structure could reflect a more meaningful neurobiological communication pattern in high dimensional space. Second, topological features with longer persistence could be assumed to convey important information about the brain network, while short ones are associated with noise. Hence, a *frequency network* which integrates the highest persistent cycles can encode the important brain connectomic information, and be used to identify the specific connectivity pattern for different APOE $\epsilon 4$ groups.

Suppose we have n frequency networks Θ for n APOE $\epsilon 4$ carriers, and m frequency networks Φ for m APOE $\epsilon 4$ non-carriers in Eq. (7). After adding the weights of every corresponding edges together for each frequency network group, we can achieve the network $\tilde{\Theta}$ or $\tilde{\Phi}$ in Eq. (8). A difference analysis is performed for each specific connectivity. Subsequently, we select a threshold ($\epsilon_t=2$) to filter the difference results and to obtain the ensuing *difference network* (binary network) $\Delta_{\epsilon 4}$ or $\Delta_{non-\epsilon 4}$ in Eq. 9. That is to say, the specific edges in network $\Delta_{\epsilon 4}$ could appear more often in the APOE $\epsilon 4$ carriers than non-carriers. Furthermore, compared to the edge measurement in $\Delta_{\epsilon 4}$ or $\Delta_{non-\epsilon 4}$, the specific loops could reflect the potential biological communication pattern. In this

Table 1 The significance (*p*-value of a two-sample t-test) of group comparison results (APOE $\epsilon 4$ carriers vs non-carriers) using six network measures from three types of brain networks

	LE	BET	GE	CCO	PH-0	PH-1
FC	0.4388	0.6570	0.9791	0.5022	0.0244	0.1562
SC	0.0947	0.4632	0.1927	0.0526	0.0081	0.0560
Proposed	0.0196	0.1469	0.2756	0.0178	0.0001	0.0321

The three types of brain networks include functional connectivity networks (FC), structural connectivity networks (SC), and the networks constructed using our proposed method (Proposed). The six network measures include local efficiency (LE), betweenness (BET), global efficiency (GE), clustering coefficient (CCO), and two PH measurements (PH-0 and PH-1)

study, we further extract the loop structures from $\Delta_{\epsilon 4}$ or $\Delta_{non-\epsilon 4}$ to quantify the APOE $\epsilon 4$ -associated connectivity.

$$\Theta = \{\Theta_1, \Theta_2, \dots, \Theta_n\}, \quad \Phi = \{\Phi_1, \Phi_2, \dots, \Phi_m\} \quad (7)$$

$$\tilde{\Theta} = \sum_{i=1}^n \Theta_i, \quad \tilde{\Phi} = \sum_{j=1}^m \Phi_j \quad (8)$$

$$\Delta_{\epsilon 4} = \tilde{\Theta} - \tilde{\Phi} < \varepsilon_t, \quad \Delta_{non-\epsilon 4} = \tilde{\Phi} - \tilde{\Theta} < \varepsilon_t. \quad (9)$$

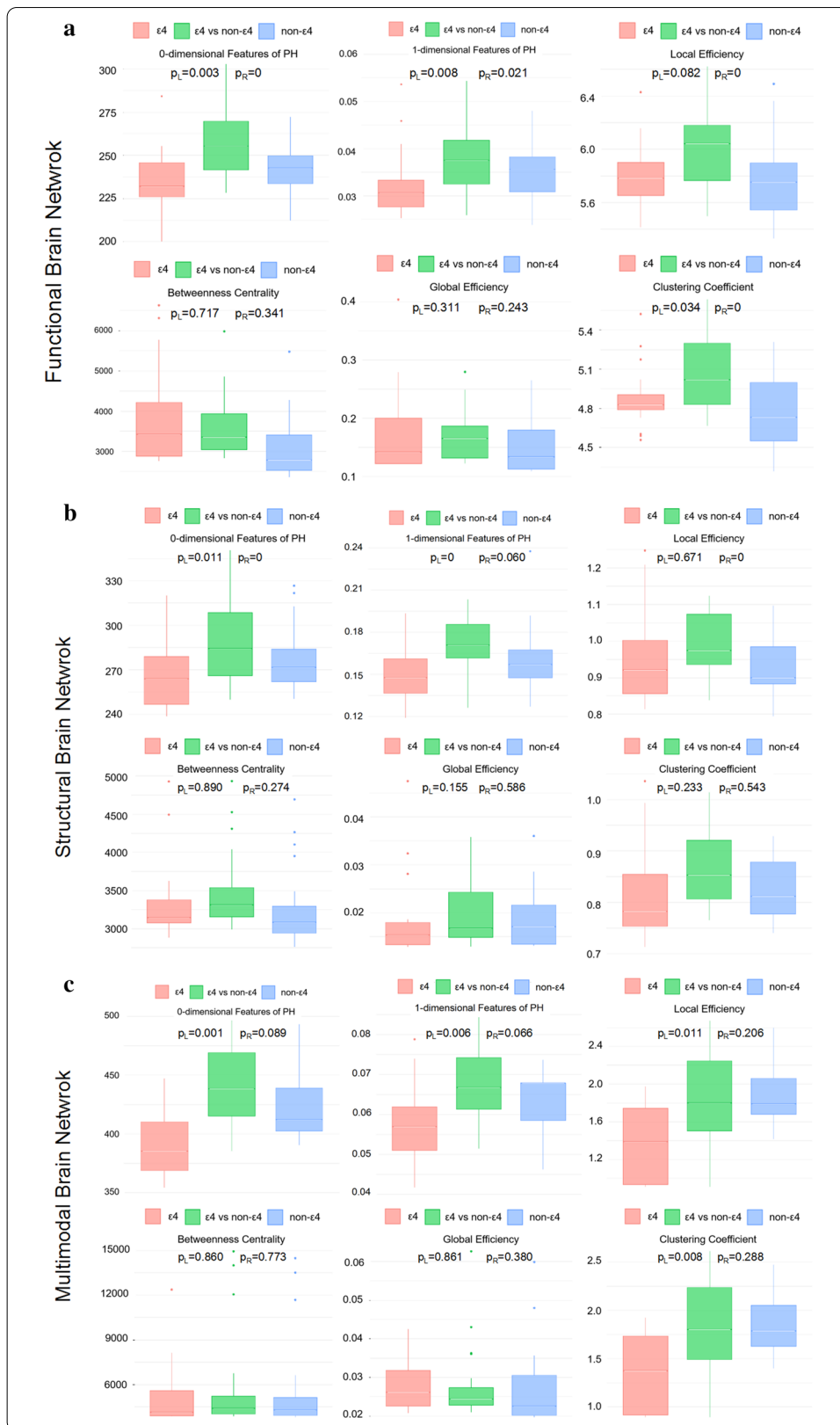
Results

Performance comparison

Table 1 shows the significance (*p*-value of two-sample t-test) of group comparison results (APOE $\epsilon 4$ carriers vs non-carriers) using six network measures from three types of brain networks. From Table 1, no statistically significant differences ($p > 0.05$) were found in terms of LE, BET, GE, CCO, and PH-1, of the whole brain FC. But a significant difference in PH-0 were observed, $p = 0.0244 < 0.05$, between APOE $\epsilon 4$ carriers and non-carriers. For the whole brain SC, one significant difference in PH-0 was found, $p = 0.0081 < 0.05$, and the groups do not differ significantly in other measurements, which is similar to FC. Of note, for the SC, *p* values is lower than that in FC, which represents a more significant difference shown in SC. Especially, PH-1 shows a significant improvement relative to that in FC, and the result is marginally significant with $p = 0.056$. For the proposed multimodal brain network, our method outperforms the competing FC and SC. The statistically significant differences were found in LE ($p = 0.0196$), CCO ($p = 0.0178$), PH-0 ($p = 0.0001$), and PH-1 ($p = 0.0321$) between groups. We further quantified the subject-wise network differences using DWG and DBG for the FC, the SC, and the multimodal network (see Fig. 3) and performed a paired t-test between neighbor columns in each

(See figure on next page.)

Fig. 3 For **a** the functional connectivity, **b** the structural connectivity, and **c** the proposed multimodal brain connectivity, the distance between groups (DBG, in green) and the distance within group (DWG, $\epsilon 4$ group in red and non- $\epsilon 4$ group in blue) are given. We compared the persistent homology features and some graph theory metrics. A discriminative feature corresponds to a large DBG (green) against two small DWGs (red and blue). In addition, p_L and p_R represent the statistical significance using t-test between any columns, i.e. DWG ($\epsilon 4$) and DBG, DWG (non- $\epsilon 4$) and DBG, respectively



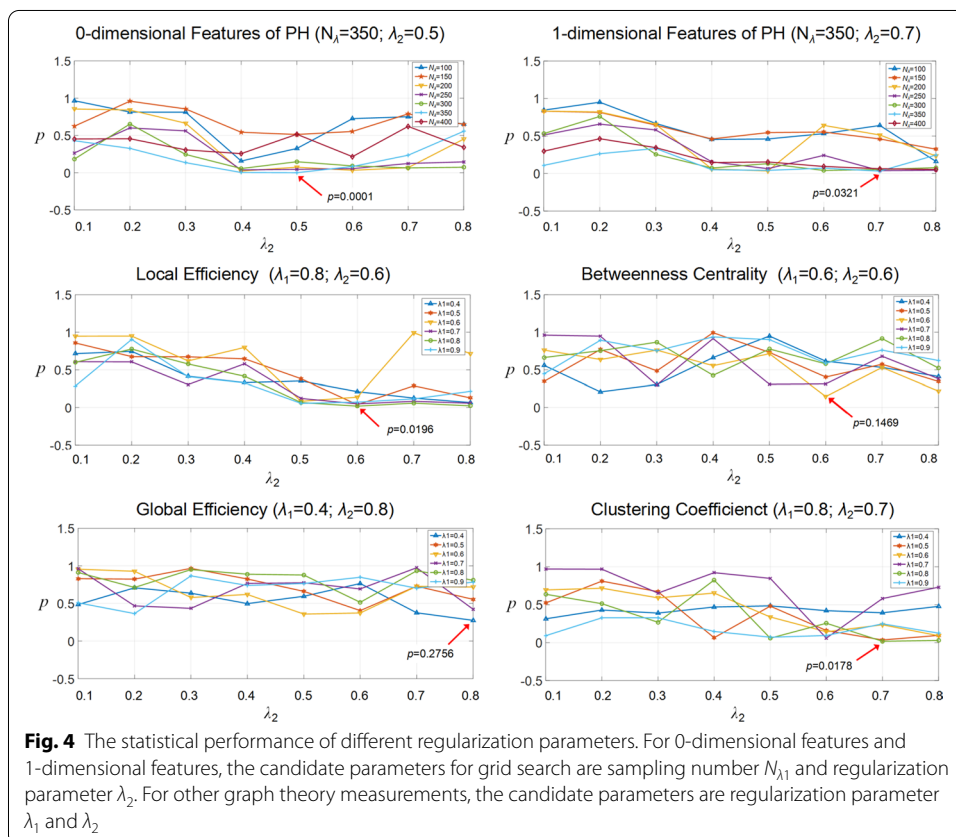
boxplot. We found that the PH metrics reflect the difference of networks better than graph metrics like LE, BET, GE, and CCO. That is to say, the DBG (green) between APOE $\epsilon 4$ carriers and non-carriers should be higher than the DWG within carriers (red) or DWG within non-carriers (blue).

The influence of regularizations

We applied grid search to explore the influence of regularizations for statistical group analysis. From Fig. 4, the performances in LE, BET, GE, and CCO are irregular, which is because graph theory measurements have a strong parametric sensitivity for network structures. In addition, we found that when N_λ is small ($N_\lambda = 100, 150, \text{ and } 200$), p values in PH-0 remain a relatively high level (lower significance level). With an increasing value of N_λ , p value achieves the best performance ($p = 0.001$) at $N_\lambda = 350$, and then shows a suboptimal performance again at $N_\lambda = 400$. For PH-1, the trend is almost similar to PH-1 that the best performance is received ($p = 0.0321$) at $N_\lambda = 350$. For λ_2 , we found p value shows a growth trend firstly, and after achieving the optimization λ_2 (0.5 and 0.7 for PH-0 and PH-1), the performance tends to decrease.

Connectivity pattern identification

After obtaining the frequency network for every subject, we constructed the difference network between groups by the proposed connectivity pattern identification framework. Furthermore, we extracted the loops from each difference network corresponding



to APOE $\epsilon 4$ group or non- $\epsilon 4$ group, where it totally has 40 loops for $\Delta_{\epsilon 4}$ and 35 loops for $\Delta_{non-\epsilon 4}$. In particular, we defined the number of edges forming the loops as a weight, and then selected the top 8 loops with the largest weights (see Additional file 1: Appendix S2). It is worth mentioning that the loop structures might not entirely appear in the brain network of each subject, but in just parts of them. Figure 5 graphically illustrates that the extracted 8 loops for APOE $\epsilon 4$ carriers and non-carriers, respectively, where the red arcs represent the connections associated with the default mode network (DMN) that has been commonly regarded as AD-pathology related. The black arcs in Fig. 5 denote the connections outside the DMN, which extends the previous studies of DMN to the whole brain level.

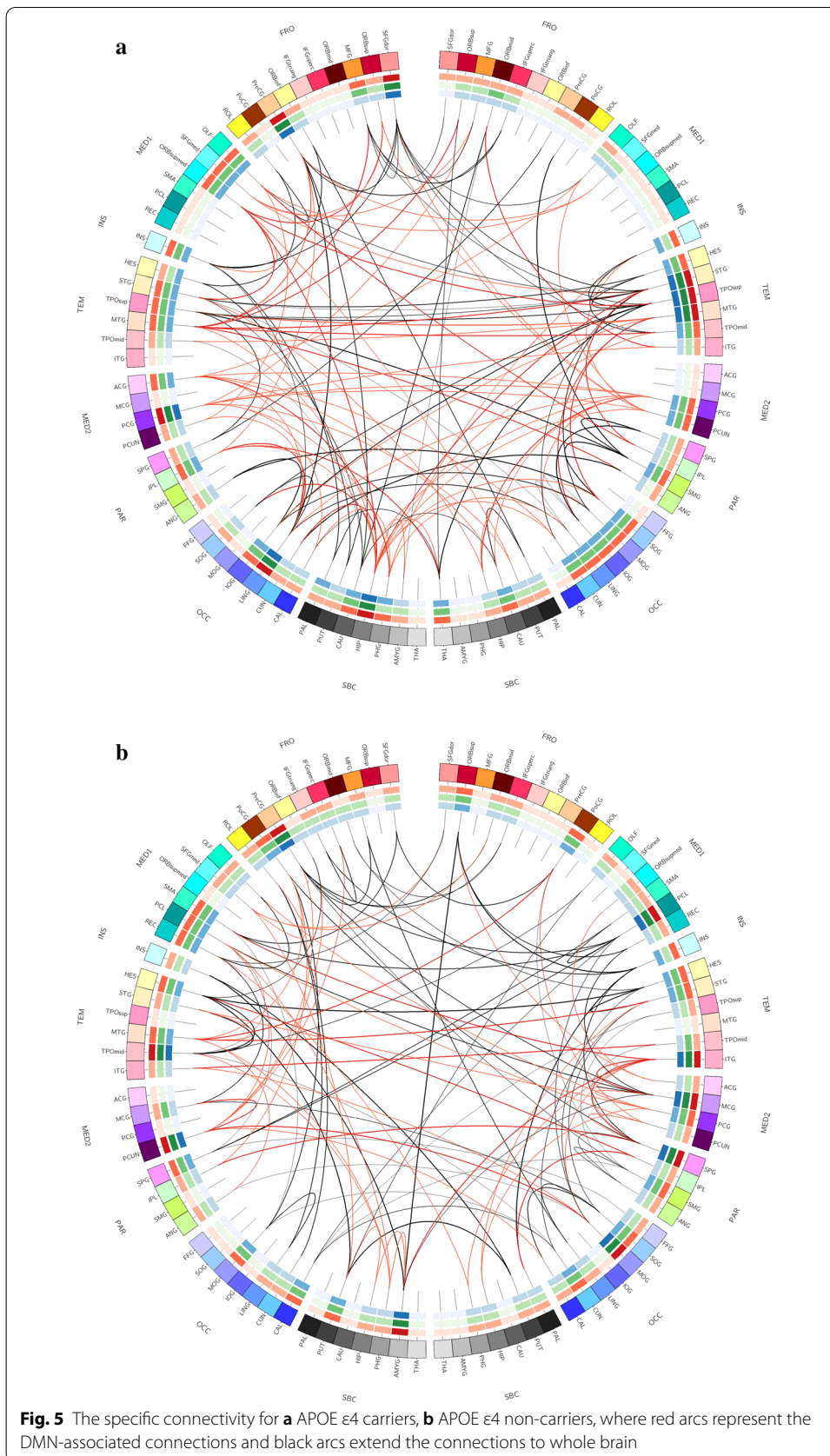
Discussion

Efficacy of the multimodal modelling

In this paper, we compared the rs-fMRI networks, the dw-MRI networks, and the multimodal networks. We found that there were no significant differences between APOE $\epsilon 4$ carriers and non-carriers in the graph measurements of the rs-fMRI and dw-MRI networks. But compared with the rs-fMRI networks, a relatively big difference was observed in the dw-MRI networks. This finding is consistent with prior studies [6, 9, 34], which found that APOE $\epsilon 4$ carriers show relatively poorer SC than FC, involving disrupted white matter microstructural organization, smaller brain volumes, and lower regional SC in DMN. Furthermore, when integrating multimodal information from the rs-fMRI and dw-MRI data using our proposed framework, we observed a significant group difference in LE, CCO, PH-0, and PH-1. Although the same significant difference is observed in PH-0 for the FC, the SC, and the multimodal network, the proposed multimodal network showed the best performance ($p=0.0001$). Our observation indicates that the multimodal network is more sensitive than either rs-fMRI or dw-MRI alone in exploring specific connectivity properties related to risk of Alzheimer's disease. This result demonstrates the advantage of multimodal integration using the dw-MRI connectivity to guide the fMRI-based network construction.

Efficacy of persistent homology

We proposed a novel framework for quantifying network features using PH. The proposed framework integrates a group of brain networks with different sparsity levels, which avoids the uncertainty of regularization parameter selection. Moreover, instead of trying to obtain an unbiased estimate of connectivity strength, our method focused on the binary network structure rather than the weight-based connectivity network. Statistically, we found persistent homology features show more significant difference than other graph theory measurements at the group level. Especially, the PH-0 outperforms the PH-1 in statistical performance, which represents the connected components is more sensitive in encoding graph filtration than the topological cycle structures. After evaluating the subject-level difference using DWG and DBG, persistent homology features showed a better discriminating power than others. It is also worth noting that the DWG of APOE $\epsilon 4$ non-carriers should be larger than the DWG of the APOE $\epsilon 4$ carriers, i.e., the blue boxplot in Fig. 3 is typically higher than the red one. This indicates that the carrier group appears more homogeneous than non-carrier group. Furthermore, the



above patterns were detected only by the multimodal network with PH quantification, but not by any other studied methods. A similar approach fusing persistent homology and sparse representation has been used by [14] for characterizing the abnormality of white matter network, but they investigated a sparse version of pair-wise ROI correlation, rather than multiple co-activated ROIs, and explore the single modality rather than multiple modalities.

Efficacy of regularizations

Brain networks corresponding to various combinations of l_1 -regularization parameter λ_1 and fused Lasso parameter λ_2 have different sparsity levels, leading to a variety of different results. The bigger the l_1 -norm regularization parameter, the lower nonzero ratio will be obtained for brain network. Different from l_1 -norm regularization parameter, the fused Lasso parameter handles the feature collinearity for improved stability. By grid search to adjust the two parameters, the best combination of parameters can improve the results of statistical analysis. This demonstrates the effectiveness of searching the parameters to characterize the APOE $\epsilon 4$ -related network difference.

The evaluation of specific connectivity

The significant decrease in brain connectivity caused by AD could modularize regional brain atrophy. On the other hand, brain regions involved in a topological cycle with long persistence are potentially located in relatively independent modules in the brain network. The *frequency network* aims to record the frequent edges in a group of cycles, because the frequent edges could connect to the atrophied brain regions in APOE $\epsilon 4$ carriers with a higher probability. The *difference network* specializes these frequent edges. We further extracted the specific loops structures from the difference network as the results of connectivity pattern identification. After evaluating these loop structures, we found brain regions in APOE $\epsilon 4$ carriers mostly refer to the interconnection within the DMN than non-carriers. Especially, we found that compared with non-carriers, APOE $\epsilon 4$ carriers exhibit one cluster involving the connections between left temporal gyrus and right temporal gyrus, mainly focusing on left middle temporal gyrus, left superior temporal gyrus, right superior temporal gyrus, right middle temporal gyrus, right inferior temporal gyrus. Moreover, APOE $\epsilon 4$ carriers show the specific connectivity within a sub-network centering on the left hippocampus, extending into left/right cuneus, left/right superior occipital gyrus, right precuneus, left Inferior parietal lobule, left middle temporal gyrus, right temporal pole middle gyrus, right superior temporal gyrus, right thalamus, and left superior frontal gyrus (medial orbital). These results were founded to be associated with brain network of APOE $\epsilon 4$ carriers in previous researches [6, 8, 35], and further indicate the effectiveness of the proposed connectivity pattern identification method.

Limitation and future directions

Of note, in this study, there are two limitations needing to be improved next for the proposed method. First, our method could identify cycles consisting of the greatly changed brain regions, rather than mildly changed regions. Because significant edges between regions as the modulator have a longer persistent interval in graph filtration,

which can be easy to observe using PH. This limitation may potentially influence the result of connectivity pattern identification. Second, a relatively small number of subjects remains a problem for statistical analysis. In the future, we will improve the performance of structure identification using a more specific brain partition and validate our framework on a larger dataset.

Conclusions

In this study, we have proposed a novel multimodal brain network modeling framework for identifying the APOE ϵ 4-related differences in the brain connectome. To integrate brain network information of different sparsity levels as well as avoid extra connectivity strength estimation, we have introduced persistent homology (PH) to quantify the individual network. Experimental results on the ADNI database demonstrated that the proposed framework could generate multimodal brain networks with great discriminative power. Moreover, the persistent homology features outperformed other measurements when quantifying APOE ϵ 4-related network differences. In addition, the specific connectivity pattern could be obtained by encoding the 1-dimensional features of PH. These specific structures were consistent with previous results in DMN and expanded DMN to whole brain connectivity. These findings suggest that the proposed method not only improves the statistical performance between APOE ϵ 4 carriers and non-carriers, but also characterizes the interaction effects between brain connectivity and APOE ϵ 4.

Supplementary information

Supplementary information accompanies this paper at <https://doi.org/10.1186/s12859-020-03877-9>.

Additional file 1. The permutation test workflow and the identified disease-specific connectivity pattern.

Abbreviations

AD: Alzheimer's disease; APOE: Apolipoprotein E; rs-fMRI: Resting state functional magnetic resonance imaging; dw-MRI: Diffusion-weighted magnetic resonance imaging; DMN: Default mode network; Lasso: Least absolute shrinkage and selection operator; PH: Persistent homology; SC: Structural connectivity; FC: Functional connectivity; TE: Echo time; TR: Repetition time; FA: Filp angle; PH-0: 0-Dimensional features of persistent homology; PH-1: 1-Dimensional features of persistent homology; LE: Local efficiency; BET: Betweenness; GE: Global efficiency; CCO: Clustering coefficient; DWG: Distances within group; DBG: Distances between groups.

Acknowledgements

Data collection and sharing for this project was funded by the Alzheimer's Disease Neuroimaging Initiative (ADNI) (National Institutes of Health Grant U01 AG024904) and DOD ADNI (Department of Defense Awarard No. W81XWH-12-2-0012). ADNI is funded by the National Institute on Aging, the National Institute of Biomedical Imaging and Bioengineering, and through generous contributions from the following: AbbVie, Alzheimer's Association; Alzheimer's Drug Discovery Foundation; Araclon Biotech; BioClinica, Inc.; Biogen; Bristol-Myers Squibb Company; CereSpir, Inc.; Eisai Inc.; Elan Pharmaceuticals, Inc.; Eli Lilly and Company; EuroImmun; F. Hoffmann-La Roche Ltd and its affiliated company Genentech, Inc.; Fujirebio; GE Healthcare; IXICO Ltd.; Janssen Alzheimer Immunotherapy Research & Development, LLC.; Johnson & Johnson Pharmaceutical Research & Development LLC.; Lumosity; Lundbeck; Merck & Co., Inc.; Meso Scale Diagnostics, LLC.; NeuroRx Research; Neurotrack Technologies; Novartis Pharmaceuticals Corporation; Pfizer Inc.; Piramal Imaging; Servier; Takeda Pharmaceutical Company; and Transition Therapeutics. The Canadian Institutes of Health Research is providing funds to support ADNI clinical sites in Canada. Private sector contributions are facilitated by the Foundation for the National Institutes of Health (www.fnih.org). The grantee organization is the Northern California Institute for Research and Education, and the study is coordinated by the Alzheimer's Disease Cooperative Study at the University of California, San Diego. ADNI data are disseminated by the Laboratory for Neuro Imaging at the University of Southern California.

Data used in preparation of this article were obtained from the Alzheimer's Disease Neuroimaging Initiative (ADNI) database (adni.loni.usc.edu). As such, the investigators within the ADNI contributed to the design and implementation of ADNI and/or provided data but did not participate in analysis or writing of this report. A complete listing of ADNI investigators can be found at: http://adni.loni.usc.edu/wp-content/uploads/how_to_apply/ADNI_Acknowledgement_List.pdf.

About this supplement

This article has been published as part of BMC Bioinformatics Volume 21 Supplement 21 2020: Accelerating Bioinformatics Research with ICIBM 2020. The full contents of the supplement are available at <https://bmcbioinformatics.biomedcentral.com/articles/supplements/volume21-supplement-21>.

Authors' contributions

JL, LS, and CB proposed the frame and designed the analysis procedures. CB and LS implemented methods and wrote an initial draft. XM and HL(1) did the literature survey and contributed to the data preparation. CB and HL(2) conducted the experiments. LS, CB, and DC commented the draft and revised the manuscript. All the authors read and approved the final manuscript. Data used in preparation of this article were obtained from the Alzheimer's Disease Neuroimaging Initiative (ADNI) database (adni.loni.usc.edu). As such, the investigators within the ADNI contributed to the design and implementation of ADNI and/or provided data but did not participate in analysis or writing of this report. All authors read and approved the final manuscript.

Funding

Publication costs are funded by the National Natural Science Foundation of China (61773134 and 61803117), the Natural Science Foundation of Heilongjiang Province of China (YQ2019F003), the Fundamental Research Funds for the Central Universities (3072020CF0402) at Harbin Engineering University. This work was also supported in part by the National Institutes of Health (R01 EB022574) at University of Pennsylvania.

Availability of data and materials

Data used in the preparation of this article were obtained from the ADNI database (adni.loni.usc.edu). The ADNI was launched in 2003 as a public-private partnership, led by Principal Investigator Michael W. Weiner, MD. The primary goal of ADNI has been to test whether serial magnetic resonance imaging (MRI), positron emission tomography (PET), other biological markers, and clinical and neuropsychological assessment can be combined to measure the progression of MCI and early AD.

Ethics approval and consent to participate

The study procedures were approved by the institutional review boards of all participating centers (https://adni.loni.usc.edu/wp-content/uploads/how_to_apply/ADNI_Acknowledgement_List.pdf), and written informed consent was obtained from all participants or their authorized representatives. Ethics approval was obtained from the institutional review boards of each institution involved: Oregon Health and Science University; University of Southern California; University of California—San Diego; University of Michigan; Mayo Clinic, Rochester; Baylor College of Medicine; Columbia University Medical Center; Washington University, St. Louis; University of Alabama at Birmingham; Mount Sinai School of Medicine; Rush University Medical Center; Wien Center; Johns Hopkins University; New York University; Duke University Medical Center; University of Pennsylvania; University of Kentucky; University of Pittsburgh; University of Rochester Medical Center; University of California, Irvine; University of Texas Southwestern Medical School; Emory University; University of Kansas, Medical Center; University of California, Los Angeles; Mayo Clinic, Jacksonville; Indiana University; Yale University School of Medicine; McGill University, Montreal-Jewish General Hospital; Sunnybrook Health Sciences, Ontario; U.B.C. Clinic for AD & Related Disorders; Cognitive Neurology—St. Joseph's, Ontario; Cleveland Clinic Lou Ruvo Center for Brain Health; Northwestern University; Premiere Research Inst (Palm Beach Neurology); Georgetown University Medical Center; Brigham and Women's Hospital; Stanford University; Banner Sun Health Research Institute; Boston University; Howard University; Case Western Reserve University; University of California, Davis—Sacramento; Neurological Care of CNY; Parkwood Hospital; University of Wisconsin; University of California, Irvine—BIC; Banner Alzheimer's Institute; Dent Neurologic Institute; Ohio State University; Albany Medical College; Hartford Hospital, Olin Neuropsychiatry Research Center; Dartmouth-Hitchcock Medical Center; Wake Forest University Health Sciences; Rhode Island Hospital; Butler Hospital; UC San Francisco; Medical University South Carolina; St. Joseph's Health Care Nathan Kline Institute; University of Iowa College of Medicine; Cornell University; and University of South Florida: USF Health Byrd Alzheimer's Institute.

Consent for publication

Not applicable.

Competing interests

The authors declare that they have no competing interests.

Author details

¹ College of Automation, Harbin Engineering University, 145 Nantong Street, Harbin 150001, Heilongjiang, China.

² School of Computer Information and Engineering, Changzhou Institute of Technology, Changzhou 213032, China.

³ Department of Biostatistics, Epidemiology and Informatics, Perelman School of Medicine, University of Pennsylvania, B306 Richards Building, 3700 Hamilton Walk, Philadelphia, PA 19104, USA.

Received: 10 November 2020 Accepted: 13 November 2020

Published: 28 December 2020

References

1. Klaassens BL, et al. Cholinergic and serotonergic modulation of resting state functional brain connectivity in Alzheimer's disease. *Neuroimage*. 2019;199:143–52.
2. Agosta F, et al. Resting state fMRI in Alzheimer's disease: beyond the default mode network. *Neurobiol Aging*. 2012;33(8):1564–78.

3. Chang YT, et al. APOE-MS4A genetic interactions are associated with executive dysfunction and network abnormality in clinically mild Alzheimer's disease. *Neurolmage Clin.* 2019;21:1.
4. Bussy A, Snider BJ, Coble D, et al. Effect of Apolipoprotein E4 on clinical, neuroimaging and biomarker measures in non-carrier participants in the Dominantly Inherited Alzheimer Network. *Neurobiol Aging.* 2019;75:42–50.
5. Andrews JR, et al. Functional-anatomic fractionation of the Brain's default network. *Neuron.* 2010;65(4):550–62.
6. Korthauer LE, Zhan L, Ajilore O, et al. Disrupted topology of the resting state structural connectome in middle-aged, APOE, $\epsilon 4$ carriers. *Neuroimage.* 2018;178:295–305.
7. Shen L, Thompson PM. Brain imaging genomics: integrated analysis and machine learning. *Proc IEEE.* 2020;108:125–62.
8. Patrizia AC, et al. Differential default mode network trajectories in asymptomatic individuals at risk for Alzheimer's disease. *Alzheimer's Dement.* 2019;15:940–50.
9. Pietzuch, et al. The influence of genetic factors and cognitive reserve on structural and functional resting-state brain networks in aging and Alzheimer's disease. *Front Aging Neurosci.* 2019;11:1.
10. Dawei W, et al. KIBRA and APOE gene variants affect brain functional network connectivity in healthy older people. *J Gerontol Ser A.* 2020;11:11.
11. Cai B, Zille P, Stephen JM, et al. Estimation of dynamic sparse connectivity patterns from resting state fMRI. *IEEE Trans Med Imaging.* 2018;37(5):1224–34.
12. Yu RP, Qiao LS, et al. Weighted graph regularized sparse brain network construction for MCI identification. *Pattern Recogn.* 2019;90:220–31.
13. Peng C, Xiaoli L, Hezi L, et al. Generalized fused group Lasso regularized multi-task feature learning for predicting cognitive outcomes in Alzheimers disease. *Comput Methods Programs Biomed.* 2018;162:19–45.
14. Chung MK, Hanson JL, Ye J, Davidson RJ, Pollak SD. Persistent homology in sparse regression and its application to brain morphometry. *IEEE Trans Med Imag.* 2015;34(9):1928–39.
15. Li Y, et al. Novel effective connectivity inference using ultra-group constrained orthogonal forward regression and elastic multilayer perceptron classifier for MCI identification. *IEEE Trans Med Imaging.* 2019;38(5):1227–39.
16. Bubenik P, Kim PT. A statistical approach to persistent homology. *Homology Homotopy and Applications.* 2007;9(2):337–62.
17. Stolz BJ, et al. Persistent homology of time-dependent functional networks constructed from coupled time series. *Chaos.* 2017;27(4):047410.
18. Kuang LQ, et al. A concise and persistent feature to study brain resting-state network dynamics: Findings from the Alzheimer's Disease Neuroimaging Initiative. *Hum Brain Mapp.* 2019;40(4):1062–81.
19. Lee H, et al. Persistent brain network homology from the perspective of dendrogram. *IEEE Trans Med Imaging.* 2012;31(12):2267–77.
20. Zhang Y, et al. Strength and similarity guided group-level brain functional network construction for MCI diagnosis. *Pattern Recogn.* 2019;88:421–30.
21. Li Y, Liu J, et al. Multimodal hyper-connectivity of functional networks using functionally-weighted LASSO for MCI classification. *Med Image Anal.* 2019;52:80–96.
22. Pinedapardo J, Bruña R, et al. Guiding functional connectivity estimation by structural connectivity in MEG: an application to discrimination of conditions of mild cognitive impairment. *Neuroimage.* 2014;101:765–77.
23. Qi S, et al. Multimodal fusion with reference: searching for joint neuromarkers of working memory deficits in schizophrenia. *IEEE Trans Med Imaging.* 2018;37(1):93–105.
24. Yan CG, et al. DPABI: data processing and analysis for (resting-state) brain imaging. *Neuroinformatics.* 2016;14(3):339–51.
25. Cui ZX, et al. PANDA: a pipeline toolbox for analyzing brain diffusion images. *Front Hum Neurosci.* 2013;7:42–52.
26. Zomorodian A, Carlsson G. Computing persistent homology. *Discrete Comput Geom.* 2005;33:249–74.
27. Xia KL. Persistent homology analysis of ion aggregations and hydrogen-bonding networks. *Phys Chem Chem Phys.* 2018;20(19):13448–60.
28. Ramsay and Silverman. *Functional data analysis.* New York: Springer; 2005.
29. Graves S, et al. *Functional data analysis.* New York: Springer; 2009.
30. Cassidy B, et al. On the reliability of individual brain activity networks. *IEEE Trans Med Imaging.* 2018;37(2):649–62.
31. Bubenik P. Statistical topological data analysis using persistence landscapes. *J Mach Learn Res.* 2015;16:77–102.
32. Bubenik P, Dlotko P. A persistence landscapes toolbox for topological statistics. *J Symb Comput.* 2017;78:91–114.
33. Bullmore ET, Sporns O. Complex brain networks: graph theoretical analysis of structural and functional systems. *Nat Rev Neurosci.* 2009;10(3):186–98.
34. Zhangjia D, et al. Disrupted structural and functional brain networks in Alzheimer's disease. *Neurobiol Aging.* 2019;75:71–82.
35. Luo X, Li K, et al. Altered effective connectivity anchored in the posterior cingulate cortex and the medial prefrontal cortex in cognitively intact elderly APOE $\epsilon 4$ carriers: a preliminary study. *Brain Imaging Behav.* 2018;13:270–82.

Publisher's Note

Springer Nature remains neutral with regard to jurisdictional claims in published maps and institutional affiliations.